ELSEVIER

Solar Energy Materials and Solar Cells 34 (1994) 347–358

Solar Energy Materials and Solar Cells

Process technology for mass production of large-area a-Si solar modules

A. Bubenzer [a,*], P. Lechner [b], H. Schade [b], H. Rübel [b]

[a] *Fachhochschule (FH) Ulm, D-89075 Ulm-Böfingen, Germany*
[b] *Phototronics Solartechnik GmbH (PST), D-85640 Putzbrunn, Germany*

Abstract

The production of large-area (0.6×1.0 m^2) modules takes place in a fully automated semiconductor line and a semi-automated panel finishing line. The a-Si deposition occurs in a multichamber reactor for parallel processing of p-, i- and n-layers which provides for flexibility in the cell design (single- and multijunction structures) without significant loss in throughput. Specific aspects of module construction, namely the properties of commercially available large-area TCO substrates, scale-up of the PECVD process, and patterning for color–neutral semitransparent modules, are discussed. The module production is now based exclusively on a-Si/a-Si tandem structures. The average power output is initially 36 W, and stabilizes around 15% below that level.

1. Introduction

Thin-film technologies employed in photovoltaics offer several attractive features, namely

- large active areas,
- thin semiconductor layers, and hence low materials consumption,
- relatively low deposition temperatures and hence application of low cost substrate materials, as well as low energy requirements for fabrication,
- integrated monolithic series connection of cells to modules.

Among the main thin-film technologies, the one based on amorphous silicon (a-Si), compared to $CuInSe_2$ (CIS) and CdTe, has already gained a significant market share, namely 26–32% [1,2].

* Corresponding author.

SSDI 0927-0248(94)00051-S

For photovoltaic applications various aspects need to be considered, that, besides the actual energy conversion efficiency, there are other factors equally important, such as

- the cost per delivered power ($\$/W_p$),
- the additional system costs,
- the costs of an alternative solution to the given project (e.g., supply of power to a remote location by grid connection versus photovoltaic power generation plus storage, or facing of a building facade by passive marble versus photovoltaic facade panels).

Presently, commercially available a-Si based large-area photovoltaic modules yield stabilized efficiencies of about 4–5%. As far as power applications are concerned, these are generally too low to compete with the crystalline technology. However, there are several specific markets, where the a-Si technology is very well suited. Not only low-power consumer products, such as battery chargers and walklights, but also automotive systems and building integrated photovoltaics, like in facades and roofs, can become a domain of the a-Si technology. Aesthetic appearance, the option for semitransparent rather than opaque modules, the monolithic series connection of cells and the flexible electrical layout can compensate for the moderate conversion efficiency in such specific applications.

Here, we describe several aspects that particularly concern the production of large-area modules. This description is based on the premises and conditions that apply to Phototronics, which started its production line in 1991.

2. Features of the production line

The present line was conceived as a pilot line to yield large-area (0.6×1.0 m^2) modules with a capacity of 1 MW/y [3]. For the substrates, float-glass coated with SnO_2 : F as transparent conductive oxide (TCO), commercially available material is being used.

The production line is divided into two sections:

- a fully automated semiconductor line that includes the a-Si and back contact deposition, preceded by the various patterning steps to generate the monolithic series connection of cells, and
- a semi-automated panel finishing line, where contacting with leads, edge treatment, glass cutting (optionally) and encapsulation are accomplished.

The semiconductor line comprises a multichamber reactor for plasma enhanced chemical vapor deposition (PECVD) of the a-Si p-, i-, and n-layers, the sputter deposition system for back contact layers, and the patterning stations to generate the series connection of cells (see Fig. 1). These equipment components are linked by a transfer system for the panels to be transported between them and to be loaded and unloaded at each station.

Central to the semiconductor line is the large-area PECVD reactor. Its design takes into account throughput, flexibility to cell design variations, quality and uniformity of the layers, and defect density level. To ascertain reproducible

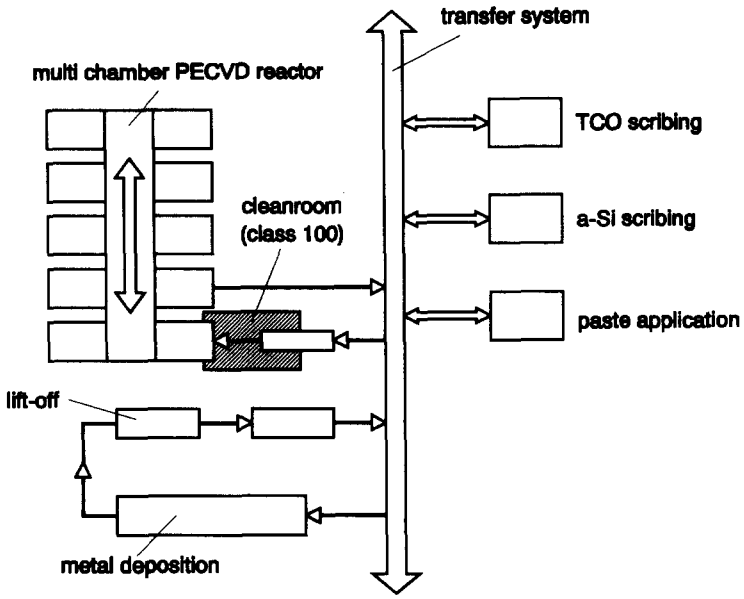

Fig. 1. Schematic view of the PECVD a-Si deposition pilot line.

high-quality i-layers and avoid potential cross contamination by dopants, a multi-chamber reactor was chosen. It consists of eight deposition chambers, two load locks for panel entry and exit, and a central transfer chamber. Unlike serial inline multi-chamber reactors, a common transfer chamber allows for parallel multi-chamber processing and, thus, for the production of double- or triple-junction devices without major losses in throughput. Each chamber is assigned only to p-, i-, or n-layers, and the duration and frequency of occupancy is governed by the respective deposition rates.

The key feature of the PECVD chambers is their plasma box design [4] which is shown in Fig. 2. The plasma box contained in each deposition chamber is separately pumped. It consists of a grounded frame and the two substrate panels pressed against it from either side to form the box covers. The double-sided RF electrode assembly is arranged central between the two substrates, with the feed gases admitted through its perforated electrode panels. This construction provides for

- plasma confinement between electrode and substrate,
- uniform deposition,
- no substrate holders being exposed to a-Si coating,
- isothermal conditions in the deposition volume,
- exclusion of wall-desorbed species by separate pumping of the plasma box and the surrounding vacuum chamber.

Furthermore, the plasma box can in-situ be easily cleaned by a plasma etching process. This procedure is crucial to avoid particles that flake off from parasitically

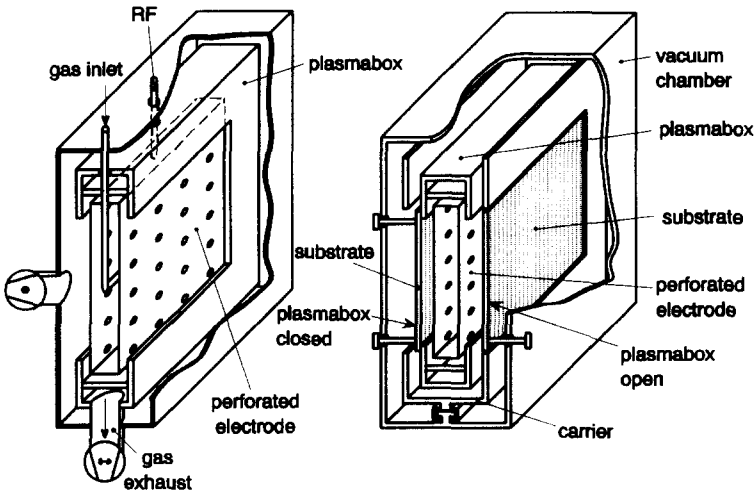

Fig. 2. Plasma box construction (schematic); shown without substrates (left), and after insertion of substrates (right).

deposited chamber walls and are a potential source for pinholes in the thin film.

The processing logistics is based on a combination of batch and in-line. While the PECVD and sputtering are in-line processes, several buffer stations between the individual process steps can bridge machine waiting periods and temporary downtimes, without stopping the processing sequence completely.

The process steps in the semiconductor line are summarized as follows (see Fig. 1). Commercially available TCO-coated glass substrates are patterned with a Nd:YAG laser. The substrates are then submitted to a fine cleaning step and transported to a small cleanroom, from where the robotic loading of the multi-chamber PECVD reactor is carried out. It should be emphasized that the sequential arrangement of substrate cleaning/loading is extremely important to attain a low pinhole density level. After deposition of the p-i-n or p-i-n/p-i-n structure, a laser scribing process for the a-Si layer as well as paste application for subsequent metal patterning by a lift-off process follow. Metal sputtering, patterning, and an electrical pretest terminate the automated part of the line.

3. Scale-up from cells to large-area modules

Having achieved equal begin-of-life efficiencies for single- and multi-junction cell structures, we exploit the superior photostability of the latter for higher end-of-life efficiencies. The cell structure consists of the layer sequence TCO/p-i-n(μc)/p-i-n/M. Both p-layers are made from a-SiC. The n-layer of the top cell is microcrystalline (μc) which provides for a low ohmic n/p contact between top and bottom cell. The back contact M consists of an Ag-based multilayer system. The cell structure does not include any buffer or bandgap-graded layers nor an

Table 1
Properties of large area TCO

Properties	Data		Correlation
	Desirable	Available	
Total transmission T_{tot} (%)	> 80	75–80	Short-circuit current I_{sc}
Diffuse transmission T_{diff} (%)	> 8	4 – 6	Short-circuit current I_{sc}
Haze = T_{diff} / T_{tot} (%)	> 10	5 – 8	Short-circuit current I_{sc}
Film resistance ($\Omega / \square$)	< 10	6 –12	Series resistance
Topography			Open-circuit voltage V_{oc} Plasma conditions → Film growth → Deposition rate Shunting p-i-n versus p-i-n/p-i-n

additional recombination layer at the n/p contact. The transition from cells to large-area modules requires aspects to be considered, that are either partly circumstantial or principal, but both equally important. Here we refer to the influence of TCO properties, and to the transfer of a-Si deposition conditions from small to large areas, respectively.

3.1. TCO substrate material

The optical, electrical, and topographical properties of the TCO material crucially influence the photovoltaic data. Both the total and diffuse transmission determine the attainable short-circuit current. In addition to governing the diffuse transmission, the kind of TCO topography may affect the growth conditions for the a-Si:H, and hence the amount of defects in the growing films, which in turn will lead to reduced open-circuit voltages. Furthermore, the sensitivity to electrical shunts is enhanced by certain topographical features, that must be avoided, particularly for p-i-n/p-i-n structures.

For large areas (0.6×1.0 m^2), TCO coatings exhibiting the various optimum properties combined are not available.

Table 1 summarizes the desired properties of TCO in comparison to those that are commercially available on large areas.

The effect of such TCO differences is illustrated in Table 2 for test cells (area 0.073 cm^2). Using optimized semiconductor depositions, as evidenced by the optoelectronic properties of the individual layers, it has not been possible to reach

Table 2
Photovoltaic data of test cells

TCO	I_{sc} (mA/cm^2)	V_{oc} (mV)	FF (%)	EFF
Asahi "U"	7.64	1.710	0.753	9.84
NSG	7.09	1.670	0.726	8.70

the 10% efficiency level with commercially available large-area substrates (here NSG), as with better optimized TCO (here Asahi "U").

3.2. PECVD process transfer

The deposition parameters cannot independently be scaled to large-area depositions to guarantee the same film properties obtained in smaller laboratory-size reactors. Although the film properties must ultimately be optimized empirically for each reactor, the anticipated changes of parameters as a function of reactor size may serve as guide lines. The interaction of these parameters must also be considered, if any changes to a given process are being contemplated. Particularly, the following parameters determine the film properties and need to be harmonized:

- Gas residence time, defined as $\tau = Vp/\phi$, where V is the plasma volume, p is the partial pressure of the gas (most importantly silane and hydrogen), and ϕ is the corresponding gas flow; τ determines the balance of reaction equilibria.
- RF power/gas flow ratio determines the silane usage for the various reaction products [5].
- Reactor symmetry, defined by the area ratio S_g/S_{RF} of the grounded and RF-powered electrode [6]; for large-area reactors ($S_g/S_{RF} < 1.5$) the energy of ionic species bombarding the substrate is increased due to the smaller electrode self-bias. Ion bombardment with excessive energies (> 70 eV) may affect the film quality [7].
- Gas utilization, defined as the ratio between deposition rate and gas flow; this ratio affects the areal uniformity of deposition. Depending on the specific gas inlet geometry, uniformity over larger areas generally requires smaller deposition rates [8].
- Plasma regime [9]; depending on the silane partial pressure, the RF power uptake of the plasma changes in its character (capacitive versus resistive). Phenomenologically, the transition to higher pressures leads to higher deposition rates and an increased tendency to powder formation (gas phase polymerization), which in turn may cause the formation of pinholes.

Due to the specificity of any given reactor, it would serve no purpose to quantitatively discuss the above parameters. Suffice it to state that the results given below were achieved with i-layer deposition rates slightly above 6 nm/min.

3.3. Cell and module efficiencies

In this context it may be useful to recall several correction factors that intrinsically account for general differences between cell and module efficiencies. These are summarized in Table 3. Thus, starting from an initial cell efficiency of 8.7% (Table 2), for large-area modules, we achieved an end-of-life aperture efficiency of 6.3%, which is within the uncertainty of the value to be expected from the correction.

Table 3
Comparison of cell and module efficiencies

	Correction	Correction factors		
		p-i-n	p-i-n/p-i-n	
Test cell "begin of life" [% c.b.o.l.]		1.0	1.0	
		[0.90]	[0.95]	
Module "active area" [% m.b.o.l. active area]	TCO resistance Lateral nonuniformity	0.90	0.95	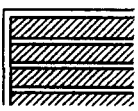
		[0.93]	[0.93]	
Module "aperture area" [% m.b.o.l. aperture]	Series connection	0.84	0.88	
		[0.75]	[0.85]	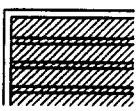
Module "end of life" [% m.e.o.l. aperture]	Stabilization (600 h AM 1, 55°C)	0.63	0.75	

4. Module-related processing

The module patterning processes are designed to be applied to both opaque and semitransparent modules. The monolithic series connection is obtained by laser scribing of the TCO and a-Si layers, and separation of the metal layer by a lift-off process. The width of the patterning lines and the line-to-line distance typically result in an area utilization of about 95%.

By adding patterning lines perpendicularly to the interconnect lines, one can create a color–neutral semi-transparency of the normally opaque module (see Fig. 3); with the correspondingly patterned metal film acting as a mask, the a-Si layers are removed. These additional lines yielding semi-transparency subdivide each cell into a number of cells that operate in parallel. The optical transmission of such modules is typically 10 to 15%, and the total power output is reduced accordingly.

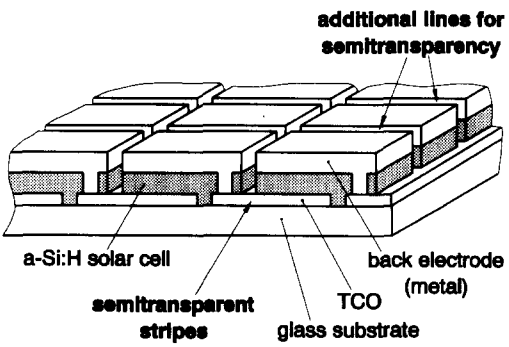

Fig. 3. Principle of series connection in the case of a semitransparent module.

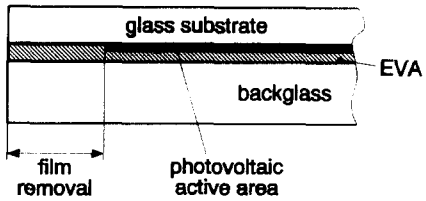

Fig. 4. Construction of a module/glass combination.

Our encapsulation process relies on a frameless glass/glass combination, where the raw module is laminated to a suitable back glass. This glass/glass combination possesses an electrical deadzone at the border (all films removed) which is resistant (non-sensitive) to corrosion (see Fig. 4).

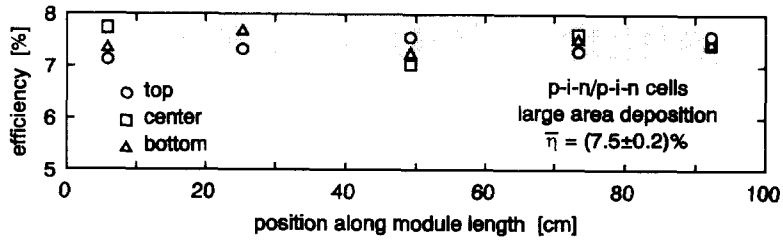

Fig. 5. Lateral variation of efficiencies of p-i-n/p-i-n tandem cells on the substrate area 0.6×1.0 m^2.

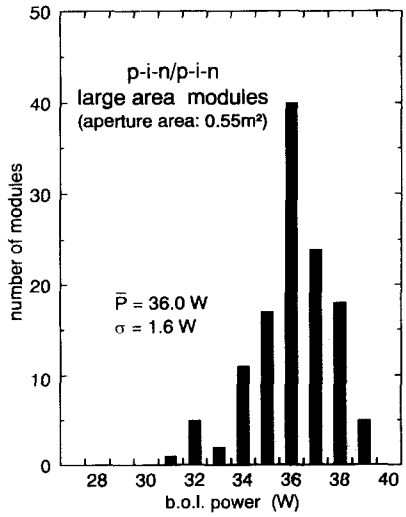

Fig. 6. Typical power distribution (begin-of-life) of 0.6×1.0 m^2 p-i-n/p-i-n modules.

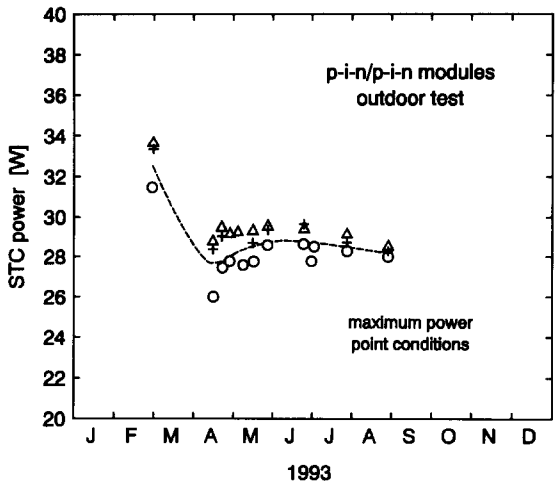

Fig. 7. The time dependence of the STC power of p-i-n/p-i-n modules (symbols for 3 different modules).

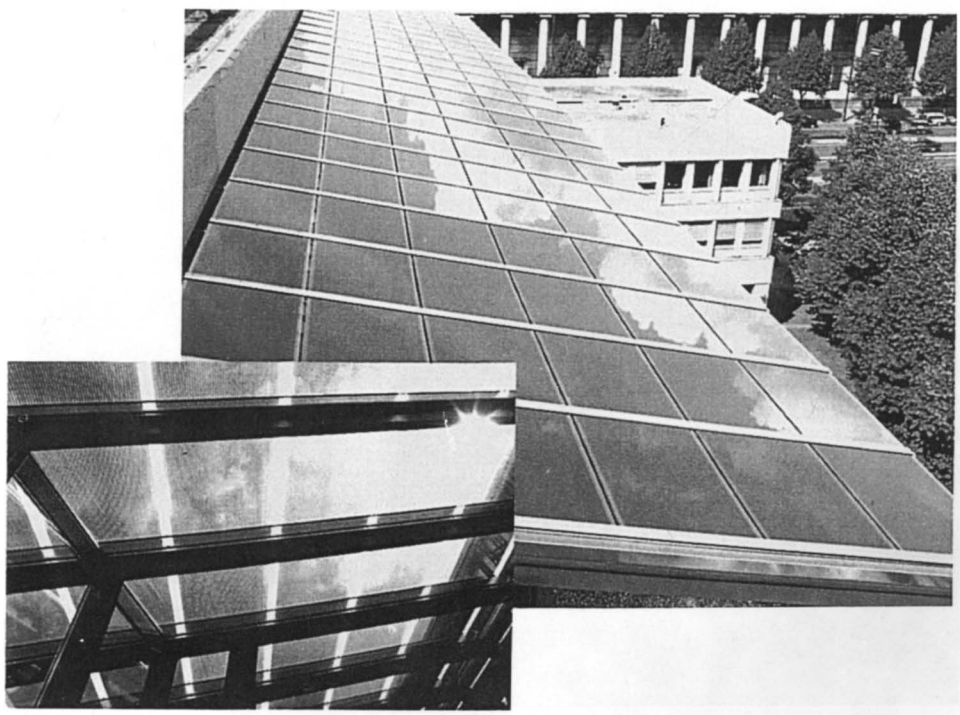

Fig. 8. Semitransparent photovoltaic roof, Office Building Bavarian State Government, Munich, Germany: 132 modules of 0.6×0.9 m^2, a-Si/a-Si tandem cell structures, color–neutral transmission 12%, 2.6 kW at 120 V dc; insert: view from inside.

5. Module performance

Initial results have been reported in Ref. [10]. The results discussed here refer to modules that are based solely on the tandem cell structure described in Section 3, and were deposited in the pilot line. The bottom i-layer thickness is 300 nm, the top i-layer has the suitable thickness for proper current matching.

The uniformity of a large-area p-i-n/p-i-n deposition is demonstrated in Fig. 5. The corresponding photovoltaic data and standard deviations of the test cells cut from a 0.6×1.0 m^2 substrate are $I_{sc} = (6.6 \pm 0.2)$ mA/cm^2, $V_{oc} = (1624 \pm 14)$ mV, FF $= (0.70 \pm 0.01)$; the total film thickness is (430 ± 40) nm.

Fig. 6 shows a typical distribution of the power outputs of large-area p-i-n/pi-n modules, measured with a Spire sun simulator. An average of (36.0 ± 1.6) W was obtained resulting from over 120 modules. The histogram in Fig. 6 gives evidence of a high reproducibility of the production processes. Based on an average

Fig. 9. Photovoltaic facade, Bavarian State Ministry for Environmental Affairs, Munich, Germany: 264 modules of 0.6×0.9 m^2, arranged in 66 panels of 4 modules each, a-Si/a-Si tandem cell structures, 6 kW at 120 V dc.

photostabilization of 15% below the begin-of-life power output, the stabilized mean aperture efficiency is 5.5%.

In Fig. 7 the outdoor testing behaviour from beginning of March to end of August of 3 modules is demonstrated. The estimated power output characteristics of the modules is corrected in terms of Standard Test Conditions (STC: 1000 W/m^2, AM 1.5, 25°C). The lowest power is reached after 6 weeks, thereafter the modules stabilize. The module temperature is around 45–50°C (20°C above ambient temperature). In these cases, the average power (32.8 W initially) is stabilizing on a level 13% below the initial power output. Under our present circumstances, these results demonstrate a distinct advantage of p-i-n/p-in module performance, compared to p-i-n single junction modules.

6. Applications

A number of features of the a-Si technology, such as large-area modules, both opaque and semitransparent, wide flexibility in available voltages due to monolithic series connection of cells, are particularly suited to specific applications that go beyond consumer products or remote energy generation.

These applications not necessarily must conform to tight energy pricing, since they serve additional functions as well. In the building industry, photovoltaic roof or facade elements not only generate electricity, but also may act as light or heat barriers, or as architecturally attractive glazing or facing.

A few examples of building-integrated photovoltaics based on the a-Si modules described here, are shown in Figs. 8 and 9.

Obviously, the realization of such projects requires the cooperation of various partners that must bring in their expertise in areas like glass laminates and patchworks, panel fixturing, and other areas normally not within the realm of photovoltaics.

Acknowledgement

This work was supported by the Bundesminister für Forschung und Technologie (BMFT).

References

[1] P.D. Maycock (Ed.), PV News 12(2) (1993).
[2] R. Curry (Ed.), Photovoltaic Insider's Report 12(2) (1993).
[3] A.M. Ricaud, J.P.M. Schmitt, J.M. Siefert, J. Méot, E. Roelen, A. Bubenzer, W. Kümmerle, W. Haüssler and M. Böttger, Proc. 10th European Photovoltaic Solar Energy Conf., Lisbon, 1991 (Kluwer Academic Publishers, Dordrecht, 1991) p. 1184.
[4] A. Bubenzer and J.P.M. Schmitt, Vacuum 41 (1990) 1957.
[5] J.R. Doyle, D.A. Doughty and A. Gallagher, J. Appl. Phys. 68 (1990) 4375.

[6] see, e.g., B. Chapman, Glow Discharge Processes (Wiley, NY, 1980) p. 165 ff.
[7] P. Roca i Cabarrocas, MRS Proc. 149 (1989) 33.
[8] J.P.M. Schmitt, MRS Proc. 219 (1991) 631.
[9] J.P. Boeuf and Ph. Belenguer, J. Appl. Phys. 71 (1992) 4751.
[10] P. Lechner, H. Schade, B. Scheppat and A. Bubenzer, Proc. 11th European Photovoltaic Solar Energy Conf., Montreux, 1992 (Harwood Academic Publishers, Switzerland, 1993) p. 568.